Chapter 10

Dynamic Tire Response to Short Road Unevennesses

Chapter Outline

The actual road surface profile over which the tire rolls may contain spectral components showing relatively short wavelengths. If the wavelength is smaller than two to three times the contact length, a geometric filtering of the profile becomes necessary if the tire model employed is assumed to contact the road in a single point.

10.1. MODEL DEVELOPMENT

For the *SWIFT* model a special filter has been developed that takes care of the envelopment properties of the tire and the variation in effective rolling radius

Tire and Vehicle Dynamics. DOI: 10.1016/B978-0-08-097016-5.00010-3

that occurs when the tire rolls over a short obstacle. The envelopment of an obstacle takes place in the contact zone. It is assumed that local dynamic effects can be neglected. The changing conditions that arise for the tire, while quasi-statically traversing an obstacle, are measured and modeled and subsequently used as effective inputs for the tire model also at higher speeds. The belt inertia takes care of the dynamic effects. The central item that is introduced is the effective road plane. Height, slopes, and curvature of the effective surface are used as inputs in the tire model. The orientation of the effective plane is defined such that the resulting force that would act on the assumedly frictionless road surface is directed normal to the effective road plane.

First, much attention will be given to developing the theory concerning rolling over two-dimensional unevennesses. Finally, rolling over three-dimensional unevennesses (such as an oblique cleat) will be addressed. In Section 10.2 model simulations are compared with experimental results.

10.1.1. Tire Envelopment Properties

In the literature one finds numerous publications on tire envelopment behavior. We refer to the study of Zegelaar (1998) for an extensive list of references. A number of these will be mentioned here. Important experimental observations have been made by Gough (1963). He indicated that the tire that is slowly rolled at constant velocity and axle height, over a cleat with length much smaller than the contact length, exhibits three distinct responses: (1) variations in the vertical force, (2) variations in the (horizontal) longitudinal force, and (3) variations in the angular velocity of the wheel. Lippmann et al. (1965,1967) studied the responses of both truck and passenger car tires rolling over short sharp unevennesses like cleats and steps of several heights. From the experimental observations it has been concluded that an almost linear relationship exists between tire force variation and step height. The superposition principle may therefore be employed to assess the response to an arbitrarily shaped unevenness by taking the sum of responses to a series of step changes in road surface height. These observations are expected to be approximately true if the obstacle height is not too large.

For three typical road unevennesses, depicted in Figure 10.1, Zegelaar has measured the responses of the tire at three different constant axle heights. To avoid dynamic effects, the velocity of the drum on which the cleat is attached (Figure 9.37) was maintained at the very low level of 0.2 km/h.

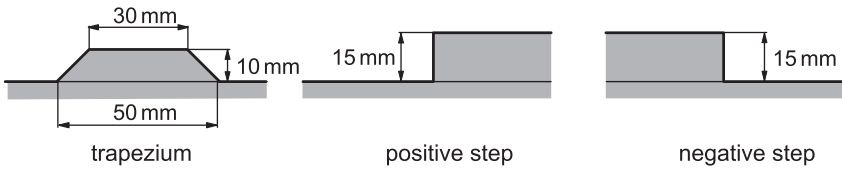

FIGURE 10.1 Three typical obstacles used in Zegelaar's research.

Figure 10.2 presents the measured vertical load F_V, horizontal longitudinal force F_H, and the effective rolling radius r_e as derived from the measurements. The latter quantity is obtained from the variation of the wheel rotation rate $d\theta/ds$, which is defined as: the difference of the incremental wheel angular

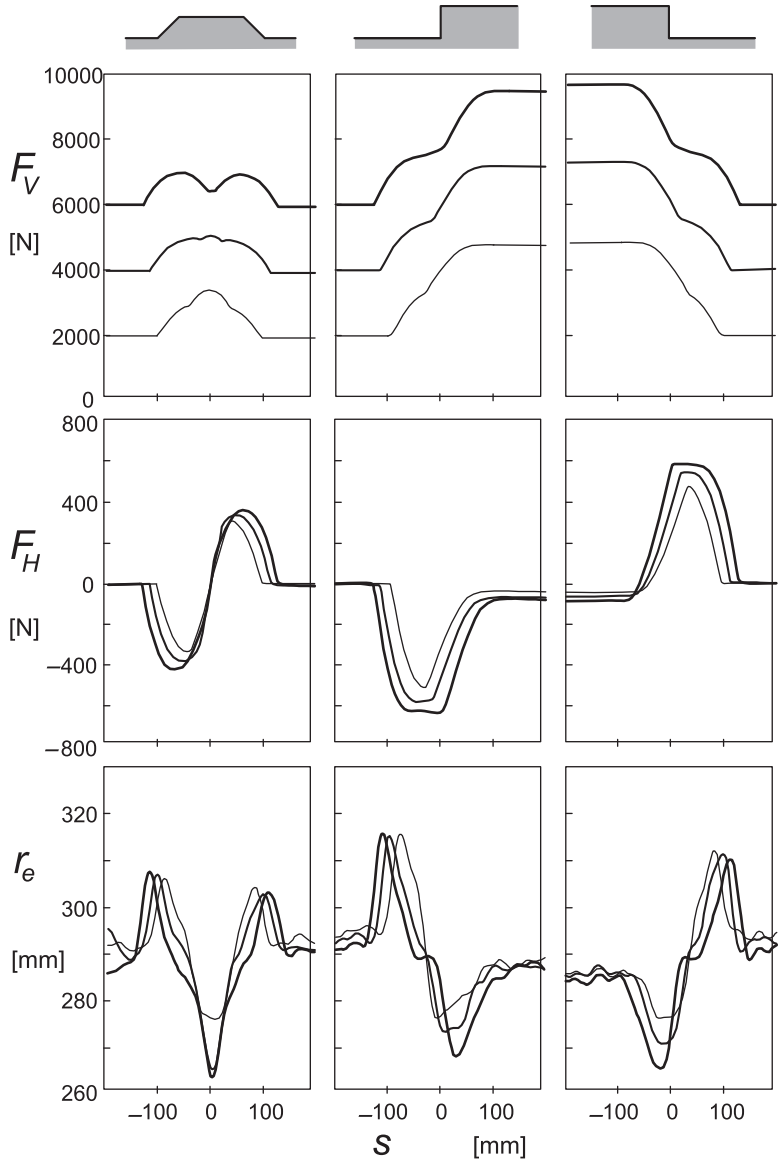

FIGURE 10.2 Rolling over a trapezium cleat, an upward, and a downward step (Figure 10.1) at very low speed and for three axle heights. Diagrams show measured variations of the vertical force F_V (upward +), the longitudinal horizontal force F_H (forward +), and the effective rolling radius r_e, Eqn (10.2). Tire dimensions: 205/60R15.

displacement and the constant (undisturbed) incremental rotation, as a ratio to the increment of the traveled distance of the wheel axle. The following equations apply:

$$r_e = \frac{V_x}{\Omega}, \qquad V_x = \frac{\mathrm{d}s}{\mathrm{d}t}, \qquad \Omega = \Omega_o - \frac{\mathrm{d}\theta}{\mathrm{d}t}, \qquad r_{eo} = \frac{V_x}{\Omega_o} \tag{10.1}$$

and hence

$$r_e \approx r_{eo}\left(1 + r_{eo}\,\frac{\mathrm{d}\theta}{\mathrm{d}t}\right) \tag{10.2}$$

The peculiar shapes of the various response curves correspond very well with results found in the literature. Several tire models have been used to simulate the experimental observations.

Davis (1974) has developed a model featuring independent radial springs distributed along the circumference. By giving the individual springs a nonlinear degressive characteristic the model is able to generate a vertical force response curve with the typical dip that shows up when running at relatively high initial loads. Badalamenti and Doyle (1988) developed a model also consisting of radial springs but now with additional interradial spring elements that connect the end points of adjacent radial springs in the radial direction. When the deflections of neighboring radial springs are not equal to each other, the interradial spring generates a radial 'shear force' that acts on the end points of the radial springs. Mousseau et al. (1994) and Oertel (1997) simulate the tire rolling over a positive step by means of (different types of) finite element models; also cf. Gipser (1987, 1999). Zegelaar uses the flexible ring (belt) model of Gong (1993) that was developed with the aid of the modal expansion method, as a reference model in his research. The addition of tread elements with radial and tangential compliances to Gong's model did enable Zegelaar to employ the model for the study of traversing obstacles. Also this model shows responses very similar to the measured behavior. Schmeitz and Pauwellussen (2001) employ the radial interradial model as a possible basis for the pragmatic model running over an arbitrary road surface.

10.1.2. The Effective Road Plane Using Basic Functions

To arrive at a geometrically filtered road profile, Bandel and Monguzzi (1988) follow the idea of Davis and introduce the effective road plane. The effective plane height and slope variation may be established by conducting an experiment where the wheel is rolled at a very low velocity over an uneven road surface at constant axle height (with respect to a horizontal reference plane) and the forces are measured, cf. Figure 10.3. It is argued that the resulting force (with the rolling resistance force omitted) that acts upon the wheel axle is directed perpendicularly to the effective road plane. By dividing the variation of

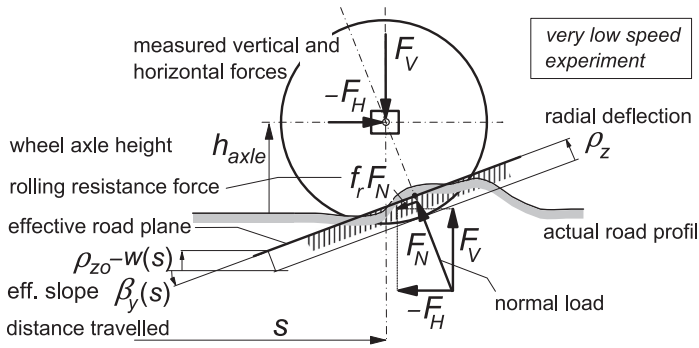

FIGURE 10.3 The wheel rolled over a road irregularity at constant axle height to establish the effective road plane variation.

the measured vertical force, which is approximately equal to the vertical component of the normal force F_N, by the radial stiffness of the tire, the effective height variation, $-w$, is obtained. The effective slope, $\tan \beta_y$, is found by dividing the longitudinal horizontal force (after having subtracted the relatively small rolling resistance force) by the vertical force. Both effective quantities are functions of the longitudinal position s of the wheel center. The following formulas apply for the effective height w:

$$-w = \frac{F_V - F_{Vo}}{C_{Fz}} \approx \frac{F_N \cos \beta_y - F_{Vo}}{C_{Fz}} = \rho_z \cos \beta_y - \rho_{zo} \tag{10.3}$$

In Section 10.1.5 a more precise definition and expression for the effective road plane height is given.

For the effective forward slope $\tan \beta_y$ we have

$$\tan \beta_y = -\frac{F_H + f_r F_N / \cos \beta_y}{F_V} \approx -\frac{F_H + f_r F_V}{F_V} \tag{10.4}$$

From Eqn (10.3) the approximate value (effect of small f_r disregarded) of the radial deflection ρ_z can be obtained. If needed, the actual effective road plane height, w' defined below the wheel spin axis, may be assessed, cf. Section 10.1.5. For the description of the effective road input the pragmatic modeling approach initiated by Bandel et al. (1988) and further developed by Zegelaar and extended by Schmeitz is most useful and will be discussed below.

The Basic Function Technique

Bandel discovered that the function representing the response of the change in vertical force to a short rectangular obstacle, featuring the dip at high load and the nipple at low load, can be decomposed into two identical basic functions, which are each other's mirror image. The basic functions are found to be

approximately independent of the initial tire vertical deflection, that is: independent of the axle height. To find the force response curve at a possibly different axle height, the basic force curves are shifted with respect to each other over a distance a bit less than the contact length and then added together. By dividing by the radial stiffness of the tire the basic height functions are found and from these the effective height variations w. For the ratio of the measured longitudinal force and vertical load variations, a pair of basic functions can be assessed as well. Again, these are identical but the first must now be subtracted from the second to find the variation of the slope of the effective road plane tan β_y, cf. Figure 10.4.

Zegelaar did experiments with the trapezium-shaped cleat, as indicated in Figure 10.1. He found basic functions, which are practically symmetric in shape. Mirror imaging was not necessary and did certainly not apply for non-symmetric unevennesses such as the step. Also, the basic functions assessed for the vertical force appeared to be practically the same as the ones for the longitudinal force. These findings helped a lot to make the principle of the basic function easier and more widely applicable. One basic function established from an experiment with a tire rolling over a given road irregularity at a fixed constant axle position should be sufficient to serve as the source for assessing the equivalent road plane height and slope. These two equivalent

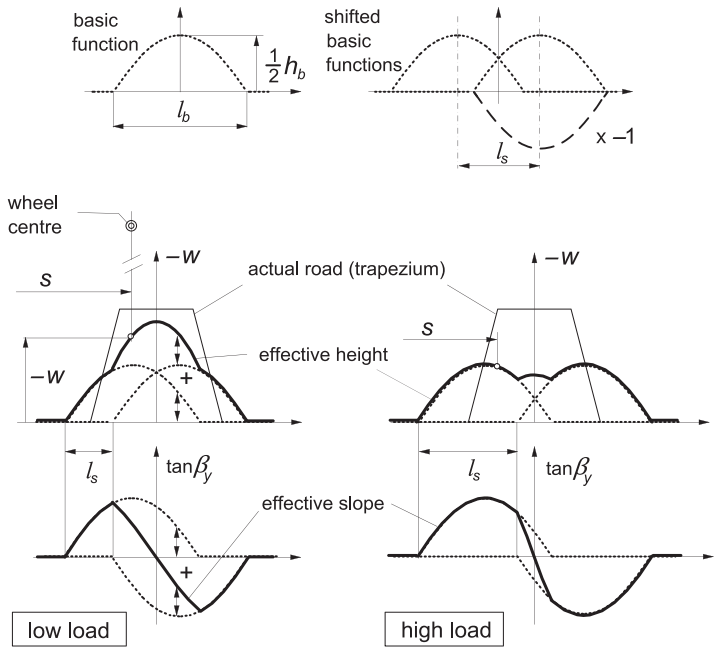

FIGURE 10.4 The construction of the curves representing the effective height and effective slope from the basic function associated with the trapezium cleat.

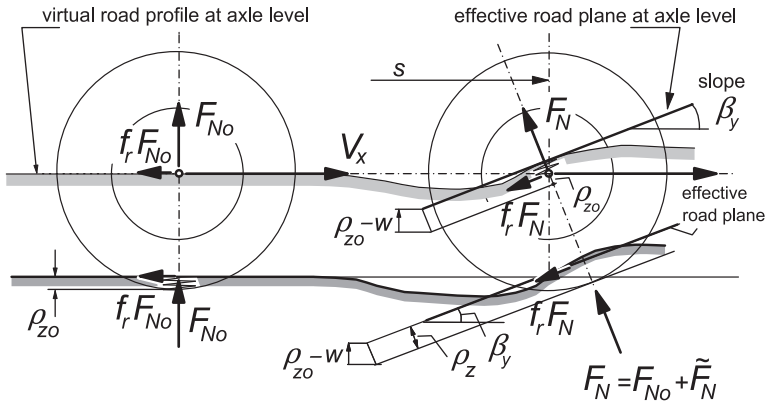

FIGURE 10.5 The virtual road profile and effective road plane as sensed at wheel axle level.

quantities will later be extended with a third quantity: the effective forward road curvature that may significantly contribute to the variation of the effective rolling radius.

Figure 10.4 demonstrates the use of the basic function for the effective height applicable for the tire rolling over a short trapezoidal cleat at a constant axle height. The vertical scale has been exaggerated. The basic function is approximated by a half sine wave. The base length of the curve is denoted with l_b, its height with $0.5h_b$, and the shift with l_s. The values of w and β_y which vary with the travelled distance s define the local effective road plane, cf. Section 10.1.5. At wheel position s the current effective road plane has been indicated. The virtual road profile defined as the path of the wheel center that would occur at constant normal load has been drawn together with the actual road profile. The distance of the wheel center with respect to the virtual road profile corresponds to the increase of the actual radial tire deflection. The distance of the wheel center to the indicated effective road plane (translated to axle level with w and β_y taken into account) is the increase in effective radial deflection that, together with the initial deflection, becomes equal to ρ_z.

The Two-Point Follower Concept

In Figure 10.6 an alternative technique is introduced using a single basic curve with full height h_b and a two-point follower. If the two points are moved along the basic curve, the midpoint describes a curve that represents the characteristic for the effective height. The inclination angle of the follower corresponds to the slope of the effective road plane.

The response to a step change in road level may serve as a building block to compose the response to an arbitrary road unevenness. The corresponding basic function may be termed as the elementary basic function. The elementary basic curve may be represented by a quarter sine wave. For the steps given in

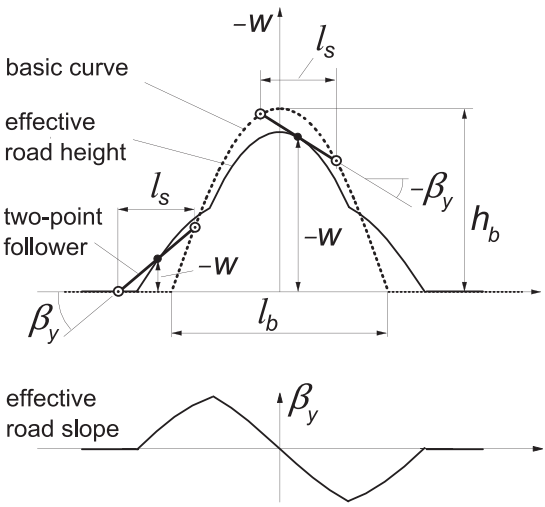

FIGURE 10.6 Alternative method to determine the effective road height and slope using the basic curve with height h_b and the two-point follower with length equal to the shift l_s.

Figure 10.1, the parameters of the basic curve have been determined by fitting the calculated force response to the vertical force variation measured for a series of axle heights (Figure 10.2).

Figure 10.7 shows the elementary basic curve for the upward step and the resulting effective road level and slope characteristics assessed by using the two-point follower technique.

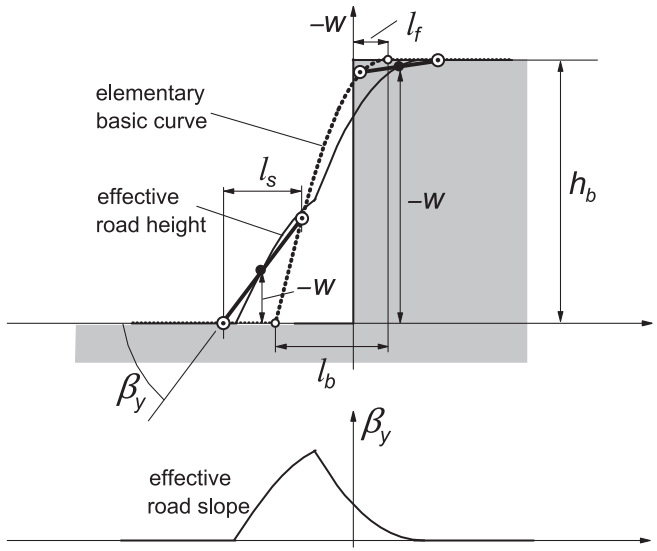

FIGURE 10.7 The effective road response curves resulting from the (elementary) basic curve associated with the step change in road level by using the two-point follower concept.

For the downward step, the fitted basic function appears to come very close to the mirror image of the one determined for the upward step. The difference may very well be neglected. The parameters that control the size and position of the basic curve are the length l_b, the shift l_s, and so-called offset l_f. The height h_b is equal to the step height. The offset is a new quantity that defines the position of the basic curve with respect to the step, cf. Figure 10.7.

A further important step is taken in the development of the assessment and use of basic functions. It is obvious that during the experiment that is performed at constant axle height, the normal load changes while rolling over an obstacle. The shift has been seen to change with axle height, that is: with a changed vertical load. The shift that corresponds to the length of the two-point follower has been found to be equal to a little less than the contact length. It seems therefore to be practical to adapt the strategy followed so far. We will henceforth define the basic curve to be assessed at constant vertical load. The experiments are to be carried out at constant load and at very low speed of travel. Schmeitz conducted such tests with the flat plank machine, cf. Section 10.2. The effective height variation follows directly from the experiment. It turns out (cf. Section 10.1.5) that w now simply equals the change in axle height, z_a. Division of the vertical force by the radial stiffness is not needed anymore, which relieves us from accounting for a possibly non-linear tire compression characteristic, cf. Eqn (9.220). In addition, since the rolling resistance is now assumed to remain constant, it is no longer necessary to take account of the rolling resistance force when determining the effective slope, as was done in Eqn (10.4).

Zegelaar calculated the step response with the flexible ring model provided with tread elements and found good agreement with measured data. By fitting the quarter sine curve representing the basic curve, parameter values have been assessed for a wide range of step heights. The results have been compared with the values calculated for a rigid wheel or zero normal load. Figure 10.8 illustrates the extreme case of the rigid wheel rolling over a step.

In Figure 10.9 Zegelaar's calculated results have been presented for a series of vertical loads F_V. The diagrams show that the basic curve length l_b and the offset l_f do change with step height h_{step} but are approximately independent of the vertical load F_V. The curve length may be estimated from the circle curve length, Figure 10.8:

$$l_b = \sqrt{r_o^2 - (r_o - h_{\text{step}})^2} \tag{10.5}$$

The horizontal shift l_s amounts to approximately 80% of the contact length $2a$. The offset may be approximated by a linear function becoming zero at vanishing step height.

The approach of employing basic curves to assess the effective road height and slope as inputs to the dynamic tire model has been found adequate for the description of the response to single obstacles. Although, in principle, the

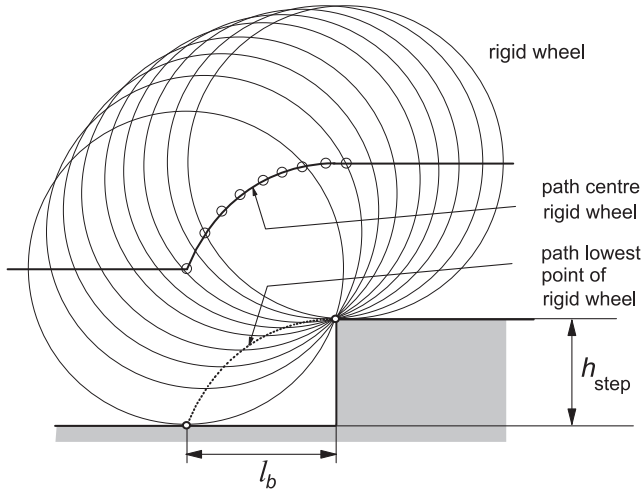

FIGURE 10.8 The rigid wheel rolling over an upward step change in road level.

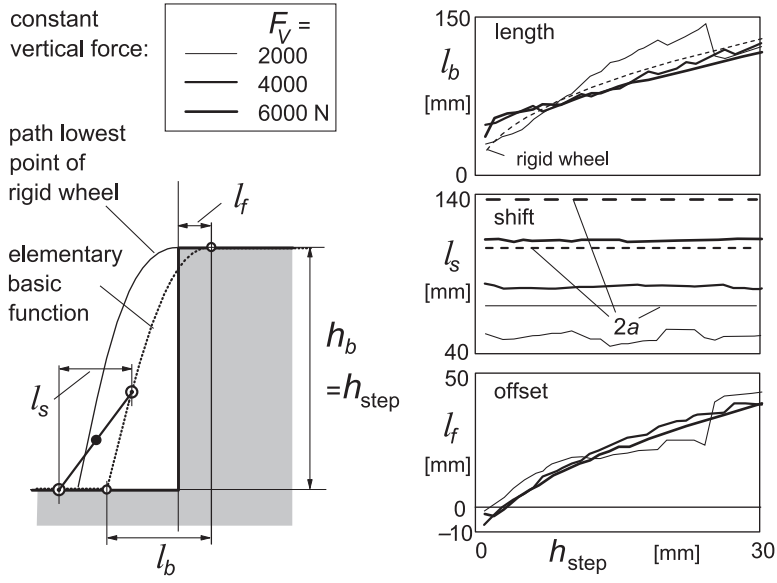

FIGURE 10.9 Parameter values for the elementary basic curve established at constant vertical loads by computations using a flexible ring model with tread elements, Zegelaar (1998).

method may be used also for a series of obstacles or for an arbitrary road surface profile with the elementary basic curve (that holds for a step unevenness) as a building block, the rules that are to be followed may become rather cumbersome. For such a more general application, the method developed by

Schmeitz (2004), also cf. Schmeitz and Pacejka (2003) based on the so-called tandem cam technique is considered to be the best option.

10.1.3. The Effective Road Plane Using the 'Cam' Road Feeler Concept

Instead of using the basic profile and running over that with the two-point follower, we may more closely consider the actual tire shape that moves over the road surface profile. Schmeitz discovered that the principle of the circle moving over the surface (Figure 10.8) may be adopted but with an ellipse instead of the circle. This super ellipse that takes the shape of a standing egg has a height approximately equal to that of the tire but a radius of curvature at the lowest point smaller than that of the free tire. In that way, the 'cam' touches the step later than the circle would. By choosing an optimal shape of the ellipse, the role of the offset l_f (that changes with step height) of the sine-based basic curve (Figure 10.9) can be taken care of automatically. Figure 10.10 depicts the cam moving over a step. The dimensions of the cam are defined by the super ellipse parameters. In terms of the coordinates x_e and z_e the ellipse equation reads

$$\left(\frac{x_e}{a_e}\right)^{c_e} + \left(\frac{z_e}{b_e}\right)^{c_e} = 1 \tag{10.6}$$

The effective road height and slope can be assessed by using two cams following each other at a distance equal to the shift length l_s. The change in height of the midpoint of the connecting line and the inclination of this line represent the effective height and effective slope, respectively.

Figure 10.11 illustrates this 'tandem cam' configuration. Fitting the tandem cam parameters follows from assessing the best approximation of low speed responses of a tire running over steps of different heights at a number of

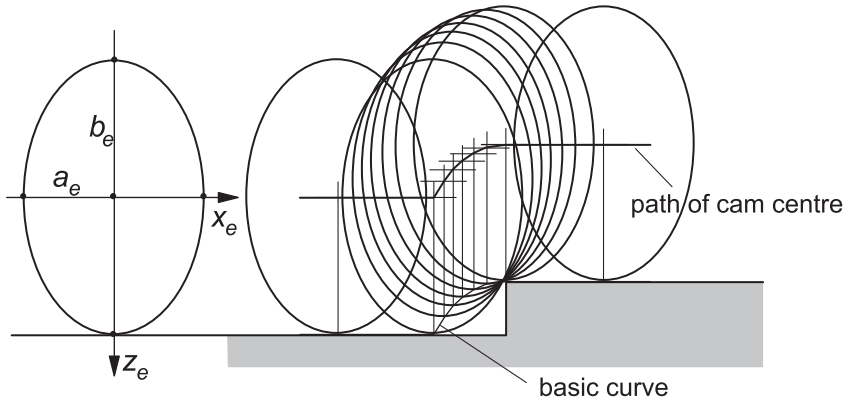

FIGURE 10.10 'Cam' moving over step road profile, producing a basic curve.

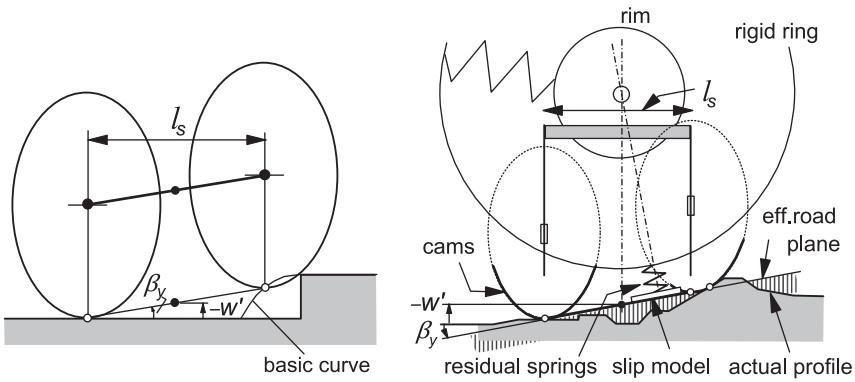

FIGURE 10.11 The tandem cam configuration that generates the (actual) effective height and slope corresponding to the use of a basic curve and two-point follower. The total model including residual spring and rigid belt ring running over an arbitrary road profile.

constant vertical loads. Once the ellipse parameters have been established, the cam dimensions can be approximately considered to be independent of step height and vertical load. The tandem base length l_s, however, does depend on the vertical load. It is interesting that analysis shows that the lower part of the ellipse turns out to be practically identical to the contour of the tire in side view just in front of the contact zone up to the height of the highest step considered in the fitting process (Schmeitz 2004).

In a vehicle simulation, it may be more efficient to assess the basic profile first, that is: before the actual wheel rolls over the road section considered. This is achieved by sending one cam ahead over a given section of the road and having that determine the basic profile. The two-point follower is subsequently moved, concurrently with the actual wheel forward motion, over the basic profile, thereby generating the (actual) effective road inputs, w' and β_y, which are fed into the tire model. Figure 10.12 illustrates the procedure. When

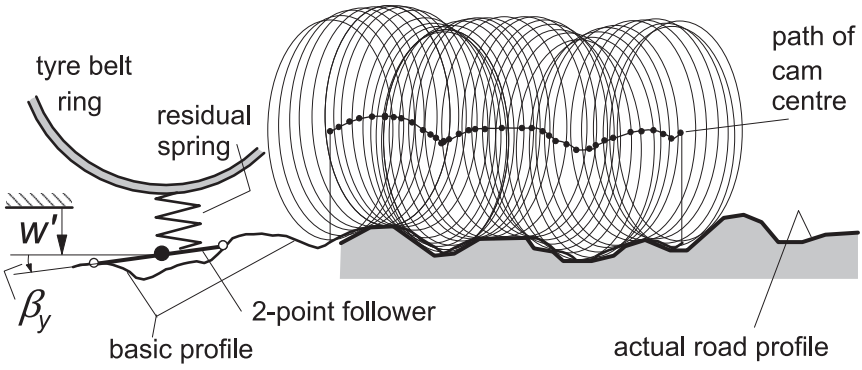

FIGURE 10.12 The cam generating the basic road profile and two-point follower moving over it.

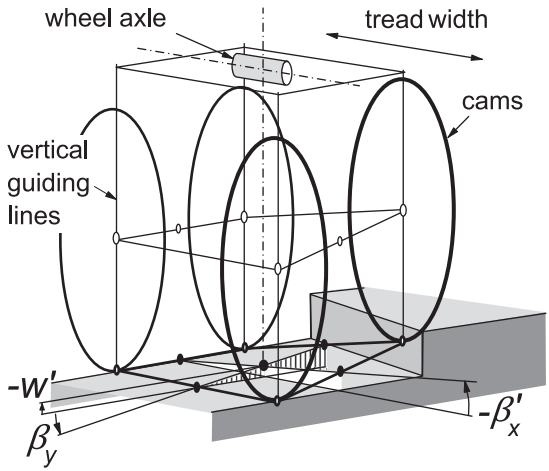

FIGURE 10.13 The double-track tandem-cam road feeler moving over an oblique step.

traversing a single step it is, of course, more efficient to use an analytic expression for the basic curve based on Eqn (10.6), cf. Figure 10.11 left.

The Double-Track Tandem-Cam Road Feeler for Road Camber Variations

For the assessment of the height and the forward and transverse slopes of the effective road plane, the double-track tandem cam road feeler will be introduced.

In Figure 10.13 the situation is depicted for an upright wheel rolling over an oblique step. The two-dimensional road feeler is used to determine the local effective two-dimensional road plane orientation in addition to the effective road plane height. See Section 10.1.5 for the slight difference between β'_x and β_x. Schmeitz has conducted extensive experimental and model studies for a tire rolling over such types of non-symmetric road unevennesses. For more information, we refer to Schmeitz (2004), and Schmeitz and Pacejka (2003). To achieve more accurate results, additional cams (say three) may be introduced along the four edges when running over non-symmetrical obstacles, such as oblique steps or strips, Figure 10.14, exhibiting transverse slope variations with short wavelength ($\lambda <$ ca. 0.2 m); see Figure 10.15.

10.1.4. The Effective Rolling Radius When Rolling Over a Cleat

The third effective input is constituted by the effective road forward curvature that significantly changes the effective rolling radius when a road unevenness is traversed. In Figure 10.2 these variations have been shown in the lower diagrams. The curves are derived from measurements by using the Eqns (10.1) and (10.2).

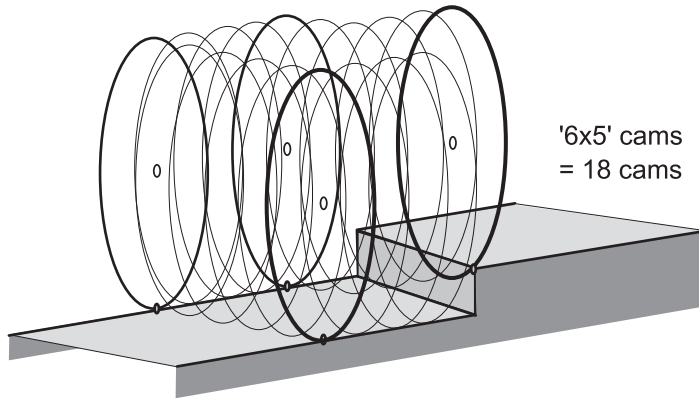

FIGURE 10.14 Road feeler with more cams on the four edges to improve accuracy.

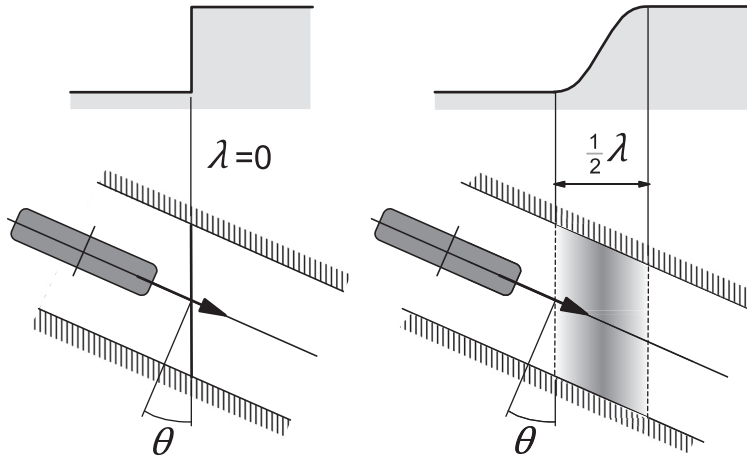

FIGURE 10.15 Oblique step with zero and larger 'wavelength'.

In the effort to model the aspect of rolling over an obstacle, it is important to realize that we have three elements that contribute to the variation of the rolling radius:

1. Increment in normal load.
2. The local forward slope.
3. The local forward curvature.

Figure 10.16 illustrates the matter. The first item has been dealt with before, cf. Section 8.3.1, Figure 8.12, and Eqn (8.38) and Eqn (9.232). According to the latter equation the effective radius is a function of vertical load and speed of rolling. In Figure 10.17, model considerations and the graph resulting from

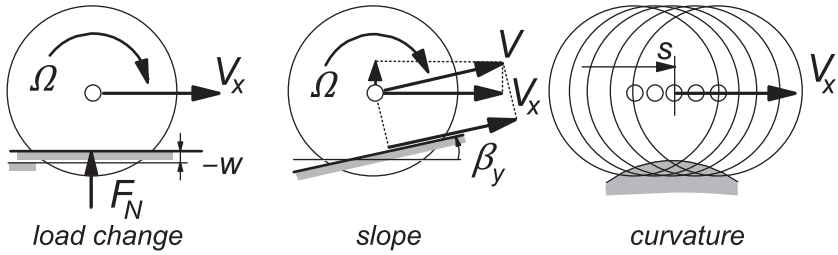

FIGURE 10.16 Three contributions to the change in apparent effective rolling radius.

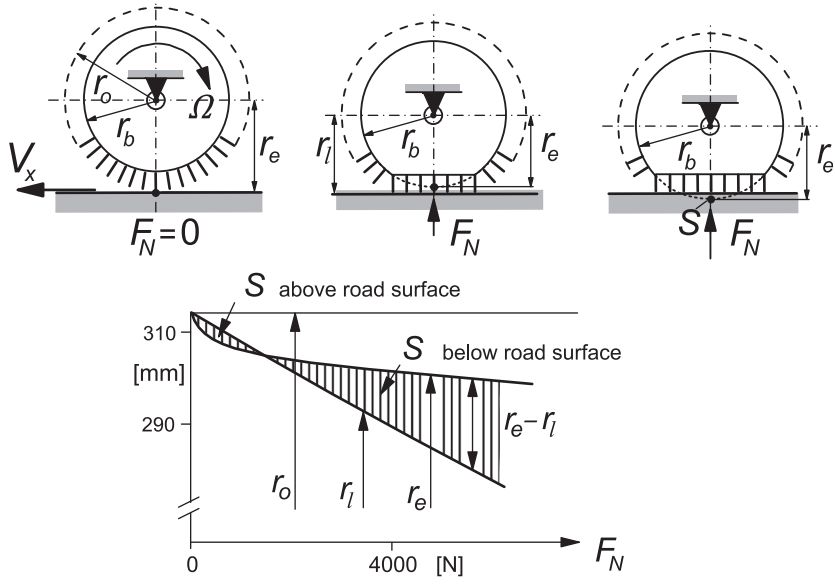

FIGURE 10.17 The effective rolling radius varying with a change in normal load.

experiments have been repeated. For small variations in radial deflection we may employ the equation

$$\tilde{r}_{e\eta} = -\eta\tilde{\rho}_z \tag{10.7}$$

The second contribution accounts for the fact that at a slope and unchanged normal load, the axle speed parallel to the road surface is larger than the horizontal component V_x. We have for the change in the apparent effective rolling radius $r_e = V_x/\Omega$

$$\tilde{r}_{e,\text{slope}} = -r_{eo}(1 - \cos\beta_y) \tag{10.8}$$

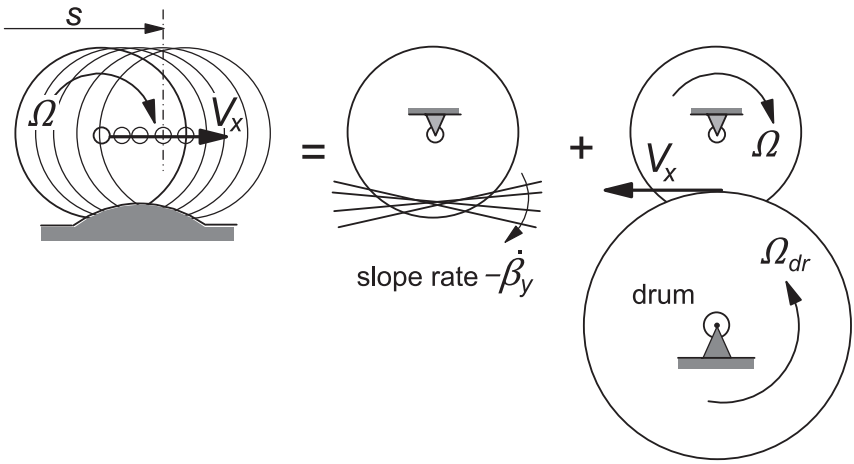

FIGURE 10.18 Unraveling the process of rolling over a curved obstacle.

The third contribution comes from the road surface curvature. The analysis that attempts to model the relation between curvature and effective rolling radius is more difficult and requires special attention. Figure 10.18 unravels the process of rolling over a curved obstacle and indicates the connection with rolling over a drum surface with same curvature. In contrast to the drum, the obstacle does not rotate. Consequently, to compare the process of rolling over a curved obstacle with that of rolling over a rotating drum surface, we must add the effect of the tire supported by a counter-rotating surface that does not move forward. The left-hand diagram of Figure 10.19 depicts a possible test configuration with a plank that can be tilted about a transverse line in the contact surface. When being tilted, point *S*, that is attached to the wheel rim, must move along with the plank in the longitudinal direction since the wheel

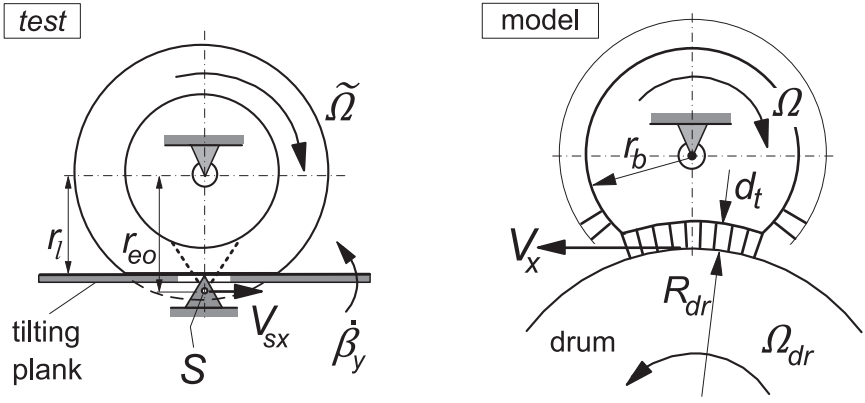

FIGURE 10.19 Two components of rolling over a curved obstacle.

slip is zero ($V_{sx} = 0$), as brake or drive torque is not applied. Consequently, the wheel rotates slightly and the following equation applies:

$$V_{sx} = -(r_{eo} - r_l)\frac{\mathrm{d}\beta_y}{\mathrm{d}t} - r_{eo}\tilde{\Omega} = 0 \tag{10.9}$$

The apparent variation in effective rolling radius derives from the equation

$$\tilde{r}_e = \frac{V_x}{\Omega} - \frac{V_x}{\Omega_o} \approx -\frac{V_x}{\Omega_o^2}\tilde{\Omega} \tag{10.10}$$

so that we obtain for the contribution from the slope rate

$$\tilde{r}_{e,\text{slope rate}} = \frac{r_{eo} - r_l}{\Omega_o}\frac{\mathrm{d}\beta_y}{\mathrm{d}t} \tag{10.11}$$

The relationship (10.9) has been confirmed to hold through elaborate experiments conducted by Zegelaar (1998) on the tilting plank of the Delft flat plank machine, cf. Figure 12.5.

The other contribution that comes from the drum analog is found by considering the simple model shown in the right-hand diagram of Figure 10.19. The tread elements with length d_t are assumed to stand perpendicularly on the drum surface. The drum has a curvature with radius R_{dr}. The belt with radius r_b is considered inextensible. As a consequence, we find the following relation between the wheel and drum velocities:

$$\Omega r_b = \Omega_{dr}(R_{dr} + d_t) = V_x\left(1 + \frac{d_t}{R_{dr}}\right) \tag{10.12}$$

and, for the effective rolling radius for the tire rolling freely over the drum surface,

$$r_{e,\text{drum}} = \frac{V_x}{\Omega} = \frac{r_b}{1 + d_t/R_{dr}} \tag{10.13}$$

For the model, the effective rolling radius of the tire rolling over a flat surface is equal to the radius of the belt:

$$r_{eo} = r_b \tag{10.14}$$

Now, the tread depth is

$$d_t = r_o - r_{eo} \tag{10.15}$$

Hence, the expression for the effective rolling radius on the drum can be rewritten as

$$r_{e,\text{drum}} = \frac{r_{eo}}{1 + (r_o - r_{eo})/R_{dr}} \approx r_{eo}\left(1 - \frac{r_o - r_{eo}}{R_{dr}}\right) \tag{10.16}$$

The variation of the radius becomes

$$\tilde{r}_{e,\text{drum}} = -(r_o - r_{eo})\,\frac{r_{eo}}{R_{dr}} \tag{10.17}$$

The drum radius is equal to the radius of curvature of the (effective) road surface profile. This curvature corresponds to change in slope β_y with traveled distance s. Note that for the convex drum surface the β_y rate of change is negative. So, we have

$$\frac{1}{R_{dr}} = -\frac{\mathrm{d}\beta_y}{\mathrm{d}s} \tag{10.18}$$

The slope rate of change may be written as

$$\frac{\mathrm{d}\beta_y}{\mathrm{d}s} = \frac{1}{V_x}\,\frac{\mathrm{d}\beta_y}{\mathrm{d}t} = \frac{1}{\Omega_o r_{eo}}\,\frac{\mathrm{d}\beta_y}{\mathrm{d}t} \tag{10.19}$$

The drum contribution is now expressed as

$$\tilde{r}_{e,\text{drum}} = \frac{r_o - r_{eo}}{\Omega_o}\,\frac{\mathrm{d}\beta_y}{\mathrm{d}t} \tag{10.20}$$

Adding up the two contributions (10.11) and (10.20) yields the variation in effective rolling radius due to obstacle forward curvature:

$$\begin{aligned}\tilde{r}_{e,\text{curvature}} &= \tilde{r}_{e,\text{slope rate}} + \tilde{r}_{e,\text{drum}} \\ &= \frac{r_o - r_l}{\Omega_o}\,\frac{\mathrm{d}\beta_y}{\mathrm{d}t} = \rho_z r_{eo}\,\frac{\mathrm{d}\beta_y}{\mathrm{d}s}\end{aligned} \tag{10.21}$$

where ρ_z is the radial compression of the tire. By adding up all the contributions, we finally obtain for the variation of the effective rolling radius with respect to the initial condition, where $\beta_y = \mathrm{d}\beta_y/\mathrm{d}s$ and $\rho_z = \rho_{zo}$:

$$\tilde{r}_e = -\eta\tilde{\rho}_z - r_{eo}(1 - \cos\beta_y) + \rho_z r_{eo}\,\frac{\mathrm{d}\beta_y}{\mathrm{d}s} \tag{10.22}$$

The term with the effective forward curvature $\mathrm{d}\beta_y/\mathrm{d}s$ constitutes by far the most important contribution to the effective rolling radius variation and thus to the wheel rotational acceleration that can only be brought about by a variation in the longitudinal force F_x. This force also often outweighs the part of the horizontal longitudinal force F_H that directly results from the slope itself, cf. Eqn (10.4).

The Five Effective Road Inputs

For the simulation of a tire rolling over an irregular road surface it turns out that, all in all, five effective road inputs are required. These are:

- The effective road plane height w'
- The effective road plane forward slope β_y

- The effective road plane transverse slope β_x
- The effective forward road curvature $\mathrm{d}\beta_y/\mathrm{d}s$
- The effective road surface warp $\mathrm{d}\beta_x/\mathrm{d}s$ (Section 10.1.5)

These effective inputs can be established with the use of the two-dimensional (multi) cam road feeler. In Section 10.2 the effective road quantities are used as inputs to the advanced dynamic tire model *SWIFT*.

If we have n cams distributed in the longitudinal direction along the total shift length L and m cams laterally along the tread width B, the calculation of the effective inputs may be indicated as follows (subscript L: left, R: right, 1: front, 2: rear; indices i (1…n) and j (1…m) start at rear and left, respectively). The height of lowest point of the individual cam is denoted with w'_{2L}, etc.:

$$\begin{aligned} w' &= \sum(w'_{1j} + w'_{2j})/2m \\ \beta_y &= \sum(w'_{2j} - w'_{1j})/mL \\ \beta_x &= \sum(w'_{Ri} - w'_{Li})/nB, \\ \mathrm{d}\beta_y/\mathrm{d}s &= \big(\beta_y(s) - \beta_y(s - \Delta s)\big)/\Delta s, \\ \mathrm{d}\beta_x/\mathrm{d}s &= (\beta_x(s) - \beta_x(s - \Delta s))/\Delta s \end{aligned} \tag{10.22a}$$

10.1.5. The Location of the Effective Road Plane

The relationship that exists between the effective height w and the actual height w' of the effective road plane has not been addressed so far. Below, a more precise account will be given of the notion of the effective road plane with a clear definition of the effective road plane height.

In Figures 10.3 and 10.5, the effective height $-w$ is considered as being assessed at a constant axle height above the reference plane that coincides with the initial flat level road surface. In Figure 10.20, the alternative case is illustrated where the effective height is assessed at constant vertical load F_V. The following formula covers both cases. The effective height is defined as

$$w = z_a - \rho_{zV} \tag{10.23}$$

where z_a denotes the vertical axle displacement and ρ_{zV} the vertical tire deflection when loaded on a flat level road with load F_V. With an assumed linear tire spring characteristic we get

$$\rho_{zV} = \frac{F_V}{C_{Fz}} \tag{10.24}$$

For the case that the effective height is found at a constant vertical load F_V, the initial vertical deflection is $z_{ao} = \rho_{zo} = \rho_{zV}$. Consequently by considering (10.24), the variation in effective height equals the change in axle height.

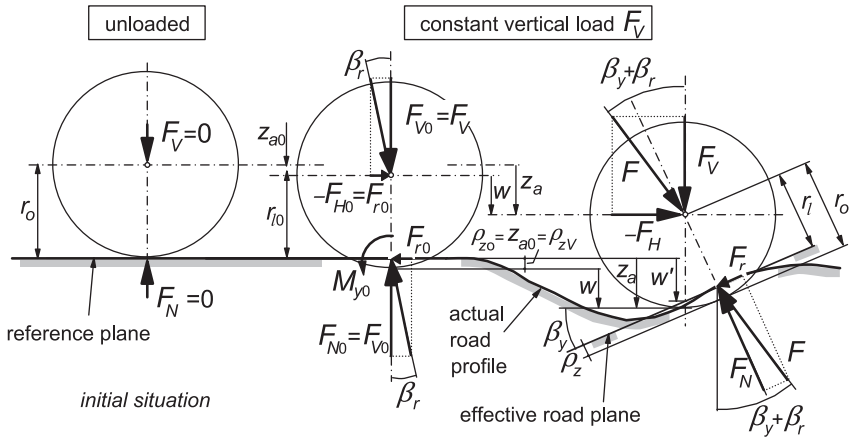

FIGURE 10.20 The effective road plane assessed at constant vertical load.

If the axle height is kept constant, we have $z_a = z_{ao} = \rho_{zo}$ and the formula becomes: $w = \rho_{zo} - \rho_{zV}$, which corresponds with Eqn (10.3).

In Figure 10.20, the actual position of the effective road plane is defined as the location of the point of intersection of effective road plane and the vertical line through the center of the vertical wheel. Its height below the horizontal reference plane is designated as w', also indicated in Figure 10.11.

With the small effect of the rolling resistance force $F_r = f_r F_N$ first included and then neglected, the normal force becomes in terms of the vertical load

$$F_N = \frac{F_v}{\cos\beta_y - f_r \sin\beta_y} \approx \frac{F_V}{\cos\beta_y} \tag{10.25}$$

Consequently, the normal deflection becomes

$$\rho_z = \frac{F_N}{C_{Fz}} = \frac{\rho_{zV}}{\cos\beta_y - f_r \sin\beta_y} \approx \frac{\rho_{zV}}{\cos\beta_y} \tag{10.26}$$

The expression for the effective road plane height w' follows from Figure 10.20 by inspection. With the vertical distance

$$z_a - w' = \frac{\rho_z}{\cos\beta_y} + r_o \frac{1 - \cos\beta_y}{\cos\beta_y} \tag{10.27}$$

we obtain, using (10.23) and (10.26)

$$w' \approx w - \rho_{zV} \tan^2\beta_y - r_o \frac{1 - \cos\beta_y}{\cos\beta_y} \tag{10.28}$$

For vanishing forward slope, we correctly find

$$w' \to w \quad \text{for} \quad \beta_y \to 0 \tag{10.29}$$

For small values of forward slope, the approximation (10.29) is perfectly acceptable.

Road and Wheel Camber

As indicated in the middle diagram of Figure 10.21, the transverse slope may be detected by a double-track tandem cam 'road feeler'. The four cams are guided along vertical lines that are positioned symmetrically with respect to the two vertical planes, one passing through the wheel spin axis and the other through the line of intersection of the wheel center plane and the horizontal plane that may be approximately defined to pass through the lowest point of the tire undeformed peripheral circle, that is at a distance equal to r_o from the wheel center.

With the effective road plane height and orientation properly defined, we have available the height w' of the point of the effective road plane vertically below the wheel center (or if needed at large camber: defined vertically above the lowest point of the undeformed tire) and the two slopes β_x and β_y. Through these quantities and the wheel axle location and orientation, the normal to the road $\boldsymbol{n}$, the loaded radius r_l, and the position vector $\boldsymbol{c}$ of C, see Section 2.2, can

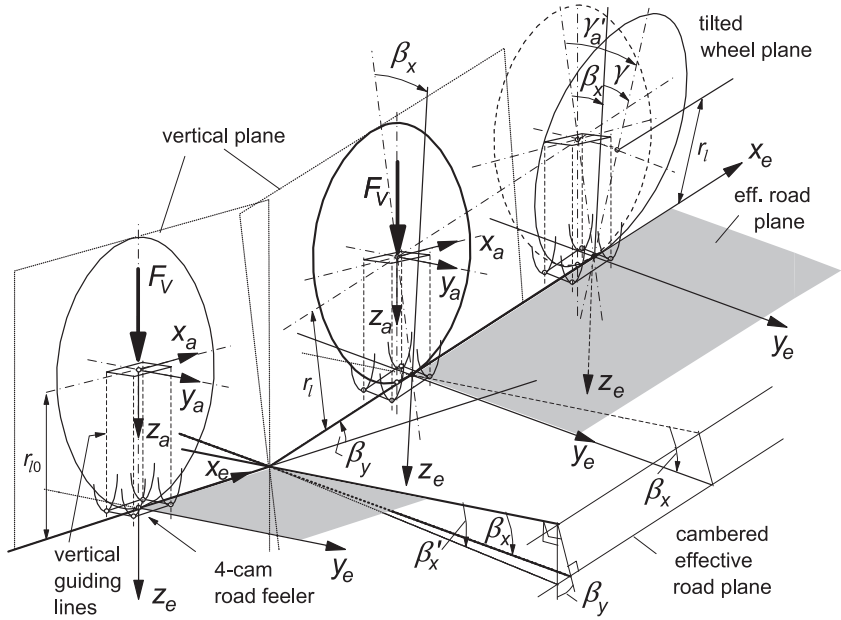

FIGURE 10.21 The effective road plane showing forward and transverse slope angles β_y and β_x. Wheel plane in the vertical and in the tilted position. Road feeler senses angles β_y and β'_x.

be assessed. With the wheel camber angle γ defined with respect to the normal to the local effective road plane and the global inclination angle γ' with respect to the vertical plane through the line of intersection ($\boldsymbol{l}$) of road plane and wheel plane, the side slip velocity V_{sy} can be calculated with Eqn (10.30). In case one is interested in the non-lagging part, Eqn (10.31) should be used as well.

The inclusion of the non-lagging part, as discussed in Section 7.2.4, is needed to get good agreement with e.g., low speed flat plank test results. The effect shows up when the effective road plane changes in height and exhibits a varying transverse slope angle β_x, cf. Figure 10.22. The expressions for the two side slip velocity components parallel to the local effective road plane (y_e axis), cf. Eqns (7.42a,b) with (7.41), now become

$$\begin{aligned} V_{sy} &= V^e_{aye} + \left(V^e_{aze} \sin\gamma - r_l \frac{\mathrm{d}\gamma^e}{\mathrm{d}t} \right) \frac{1}{\cos\gamma} \\ &= V_{aye} + \left(V_{aze} \sin\gamma - r_l \frac{\mathrm{d}\gamma'}{\mathrm{d}t} \right) \frac{1}{\cos\gamma} \end{aligned} \tag{10.30}$$

$$\begin{aligned} V_{sy1} &= V^e_{aye} - r_{sy} \frac{\mathrm{d}\gamma^e}{\mathrm{d}t} \cos\gamma \\ &= V_{aye} - \left\{ r_{sy} \frac{\mathrm{d}\gamma'}{\mathrm{d}t} + (r_l - r_{sy}) \frac{\mathrm{d}\beta_x}{\mathrm{d}t} \right\} \cos\gamma \end{aligned} \tag{10.31}$$

where $\mathrm{d}\gamma'/\mathrm{d}t$ is the time rate of change of the wheel global tilt angle. The quantities V_{aye} and V_{aze} represent the components of the global axle velocity parallel to the system of current effective road axes (x_e, y_e, z_e). Furthermore, $\mathrm{d}\gamma^e/\mathrm{d}t = \mathrm{d}\gamma'/\mathrm{d}t - \mathrm{d}\beta_x/\mathrm{d}t$ and V^e_{aye} and V^e_{aze} represent the sum of V_{aye} and V_{aze} and the components of the velocity of the virtual axle motion (due to $\mathrm{d}\beta_x/\mathrm{d}t$) relative to ($x_e$, y_e, z_e) and parallel to this system of axes. The necessity for including the last term of (10.31) becomes clear when considering the case

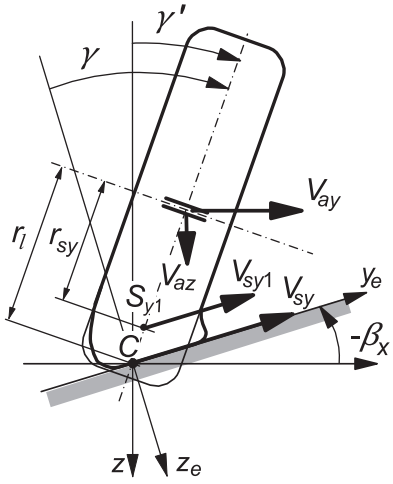

FIGURE 10.22 Side slip velocity components at road and wheel camber.

that $V_{ay,z}$ and $d\gamma'/dt$ remain equal to zero. This situation corresponds with the right-hand case C depicted in Figure 7.13. It may be noted that $d\beta_x/dt = V_x d\beta_x/ds$, with $d\beta_x/ds$ representing the effective warp of the road surface along the forward axis.

10.2. *SWIFT* ON ROAD UNEVENNESSES (SIMULATION AND EXPERIMENT)

Zegelaar and Schmeitz have performed numerous experiments on the drum test stand (Figure 9.37) and the flat plank machine (Figures 10.23 and 12.6) and used the *SWIFT* model (including enveloping model based on the effective road plane concept) to carry out the simulations.

10.2.1. Two-Dimensional Unevennesses

Figure 10.9 shows the obstacle parameter values for the quarter sine basic curve of Zegelaar. Table 10.1 gives the parameters used by Schmeitz, which are based on the ellipse concept (tandem cam technique). The table shows that the height

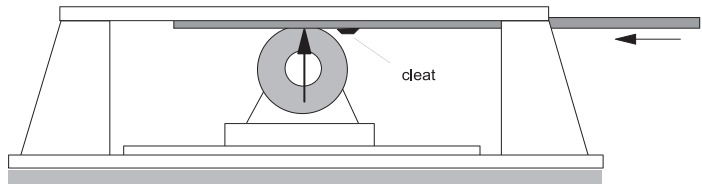

FIGURE 10.23 Principle of the flat plank machine provided with a trapezium shaped cleat.

TABLE 10.1 Parameter Values Used for Envelopment Calculations. Tire: 205/60R15, 2.2bar

unloaded radius	r_o	0.310 m
effective rolling radius at $F_N = 4000$ N	r_{eo}	0.305 m
slope effective rolling radius characteristic	η	0.3
vertical tire stiffness at $F_N = 4000$ N	C_{Fz}	220 N/mm
rolling resistance, cf. Eqns (9.230, 9.231), $f_r = q_{sy1}$	q_{sy1}	0.01
half contact length, cf. Eqn (9.207)	a	cf. Table 9.3
half ellipse length/unloaded radius a_e/r_o	p_{ae}	1.0325
half ellipse height/unloaded radius b_e/r_o	p_{be}	1.0306
ellipse exponent c_e	p_{ce}	1.8230

and length of the ellipse are slightly larger than the dimensions of the free tire. It is the exponent that gives rise to the larger curvature of the ellipse near the ground.

Figure 10.24 presents the measured and calculated variations of the effective height w (equal to the variations of the vertical axle displacement z_a at

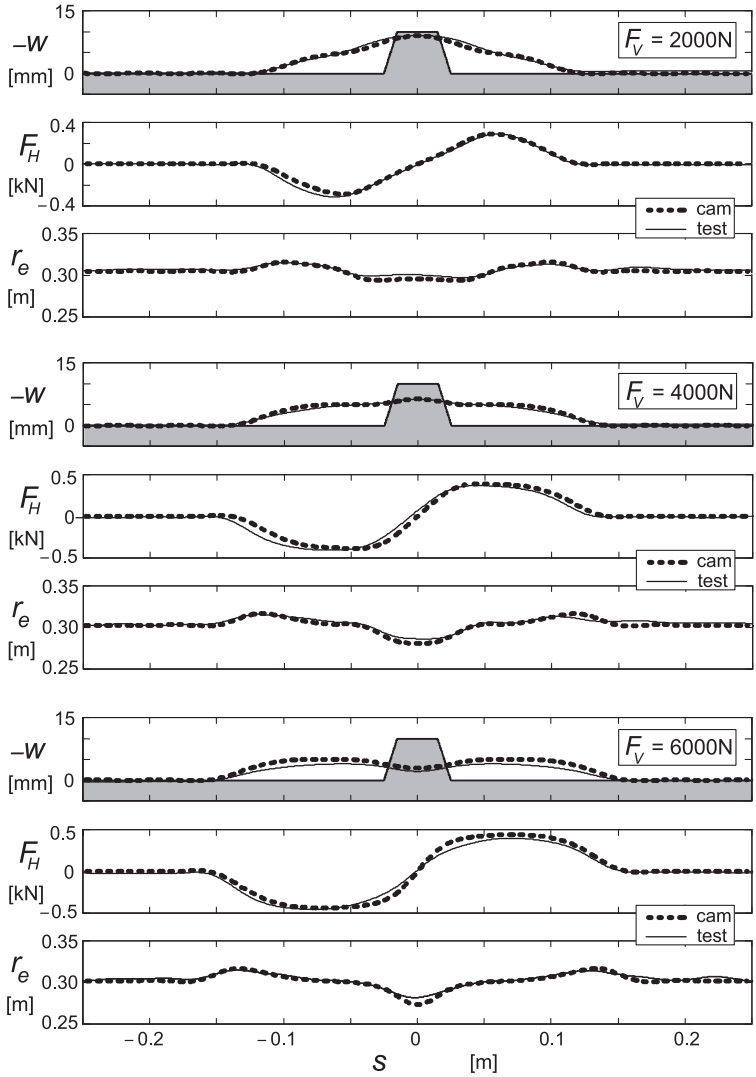

FIGURE 10.24 Rolling over a trapezium cleat (length: 50 mm, height: 10 mm). Measured and calculated variation of vertical axle displacement ($\Delta z_a = w$), horizontal longitudinal force, and effective rolling radius at three different constant vertical loads. Measurements carried out on the Delft flat plank machine (very low speed) and calculations conducted with the use of the tandem cam technique (Figure 10.11) and Eqn (10.22). Tandem cam parameters according to Table 10.1.

constant vertical load F_V), the horizontal fore-and-aft force F_H, and the effective rolling radius r_e, with the vertical load kept constant while slowly rolling over the trapezium cleat. The effective road plane slope tan β_y follows from the ratio of the horizontal force variation and the vertical load. The calculations are based on the two-cam tandem concept of Figure 10.11. The tandem is moved over the original road profile and the effective height and slope are obtained. From the derivative of β_y, the effective rolling radius is found by using Eqn (10.23), which also contains the two very small additional contributions. It is observed that a good agreement between test and calculation results can be achieved. The use of the quarter sine basic curve function gives very similar results.

Figures 10.25–10.29 present the results of rolling over the same cleat at different speeds while the axle location is kept fixed. The responses of the vertical, fore, and aft forces and the wheel angular speed have been indicated. In addition, the power spectra of these quantities have been shown.

Especially at the higher loads the calculated responses appear to follow the measured characteristics quite well up to frequencies around 50 Hz or higher. Figure 10.30 demonstrates the application to a more general road surface

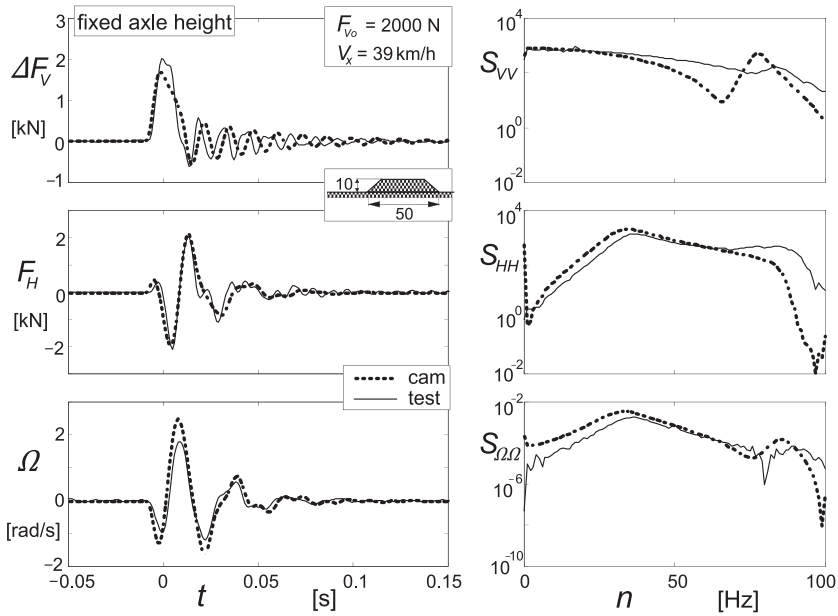

FIGURE 10.25 Time traces and power spectra of vertical, horizontal, and longitudinal force and angular velocity for wheel running at given speed of 39 km/h and initial vertical load of 2000 N over a trapezium cleat at constant axle height using *SWIFT* tire parameters and obstacle parameters of Table 10.1. (Schmeitz).

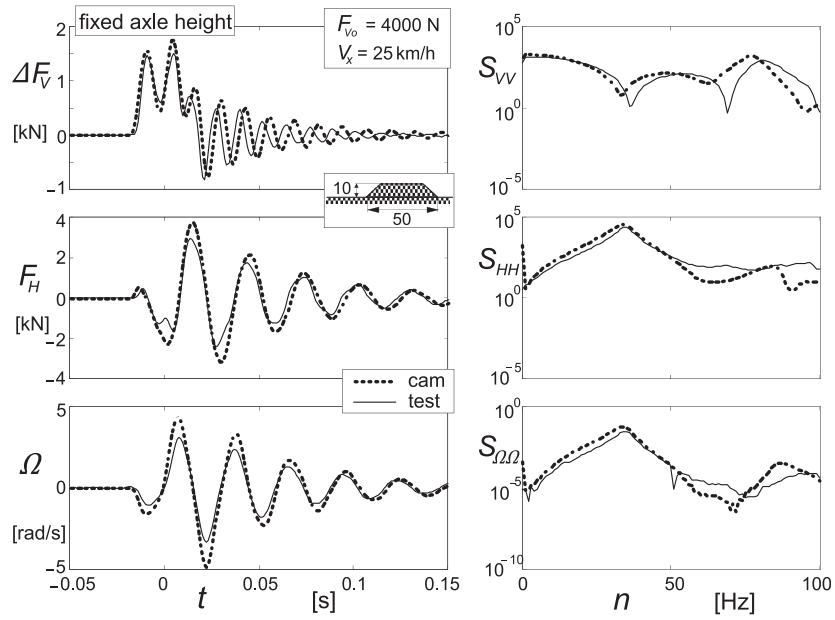

FIGURE 10.26 Same as Figure 10.25 but at different speed and initial vertical load.

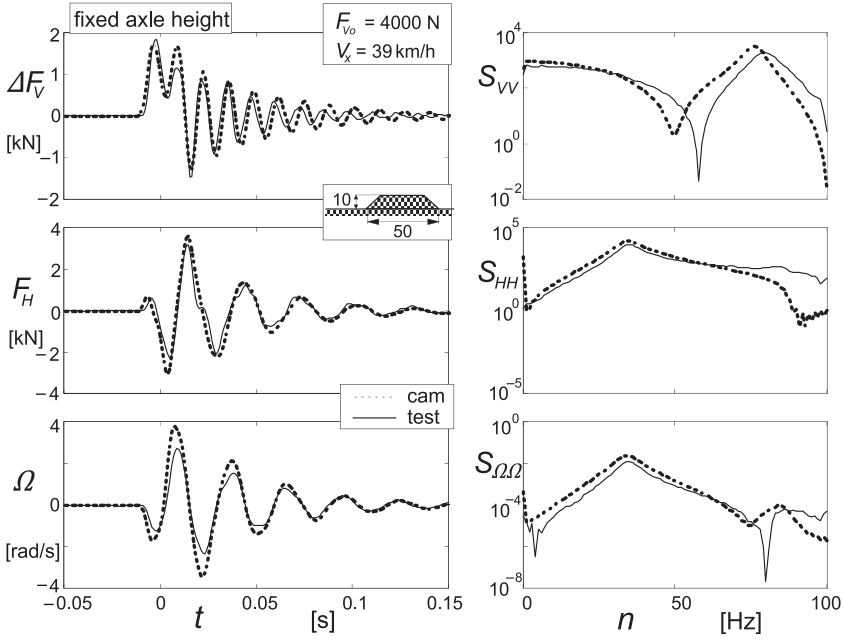

FIGURE 10.27 Same as Figure 10.26 but at higher speed.

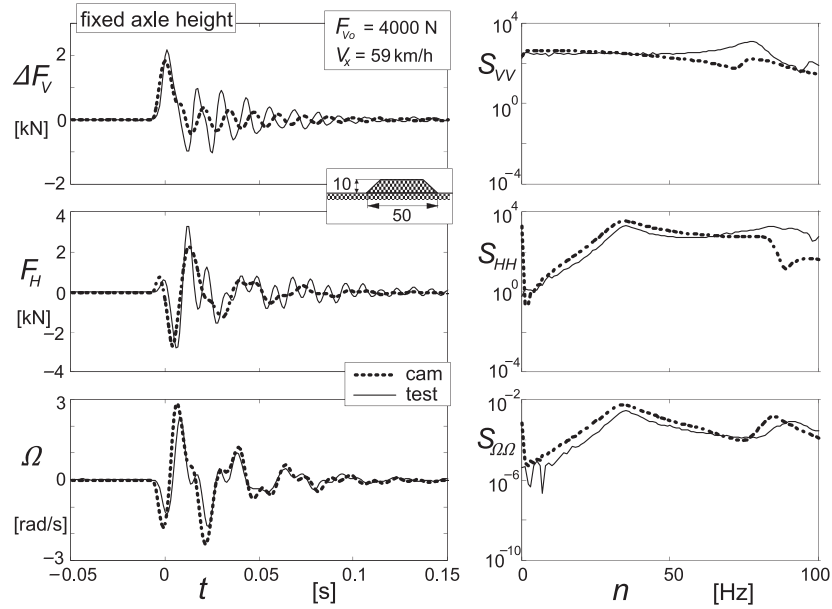

FIGURE 10.28 Same as Figure 10.27 but at higher speed.

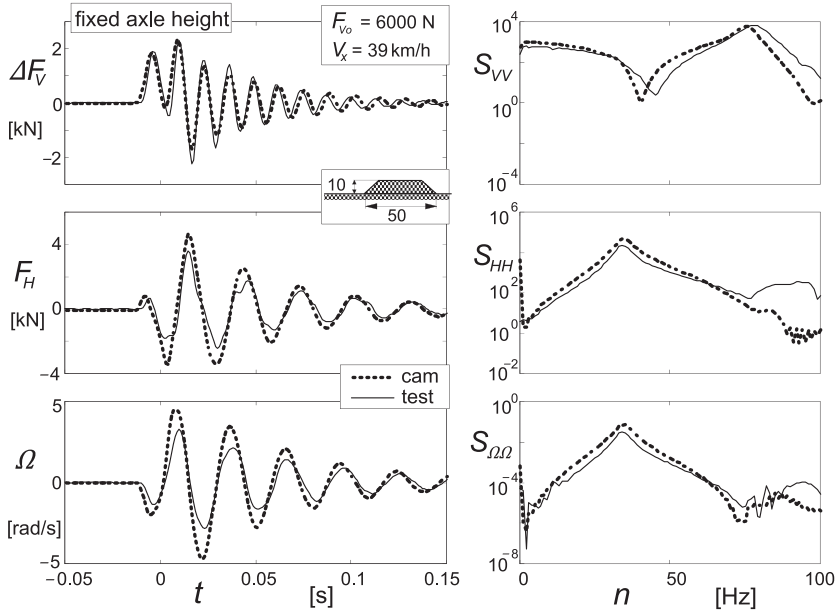

FIGURE 10.29 Same as Figure 10.27 but at higher initial vertical load.

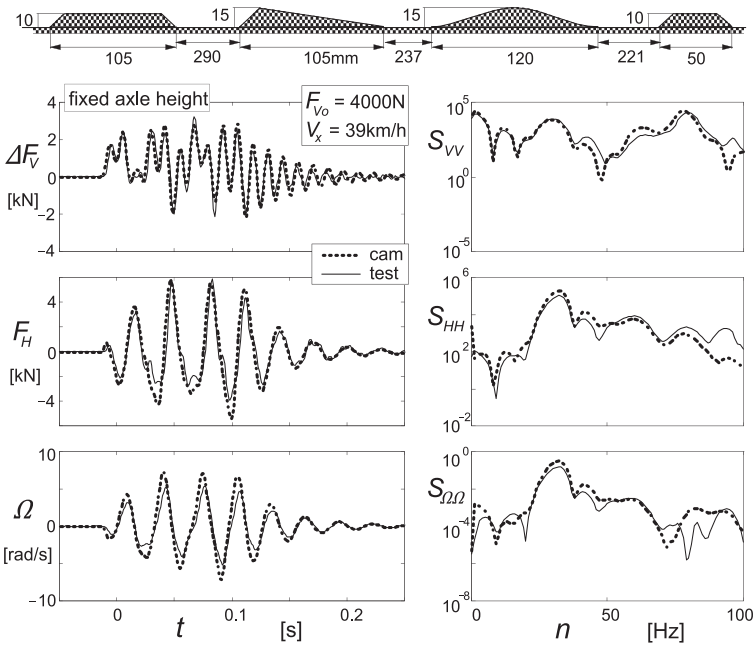

FIGURE 10.30 Running over a series of cleats mounted on drum surface, at constant axle height.

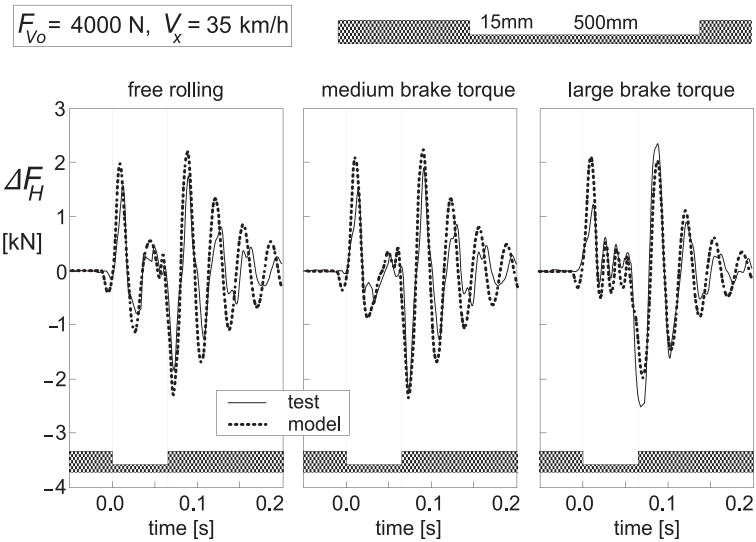

FIGURE 10.31 The horizontal force variation when traversing a pothole while the wheel is being braked at three different levels of brake torque (M_B = ca. 4, 375, 850 Nm respectively, Zegelaar 1998). Experiments on 2.5 m drum, calculations using parameters according to Figure 10.9.

profile. It shows the responses of the tire when moving over a series of different types of cleats that resembles an uneven stretch of road.

Finally, in Figure 10.31 the test and simulation results conducted by Zegelaar (1998) have been depicted, representing a more complex condition where the tire is subjected to a given brake torque (brake pressure) while the

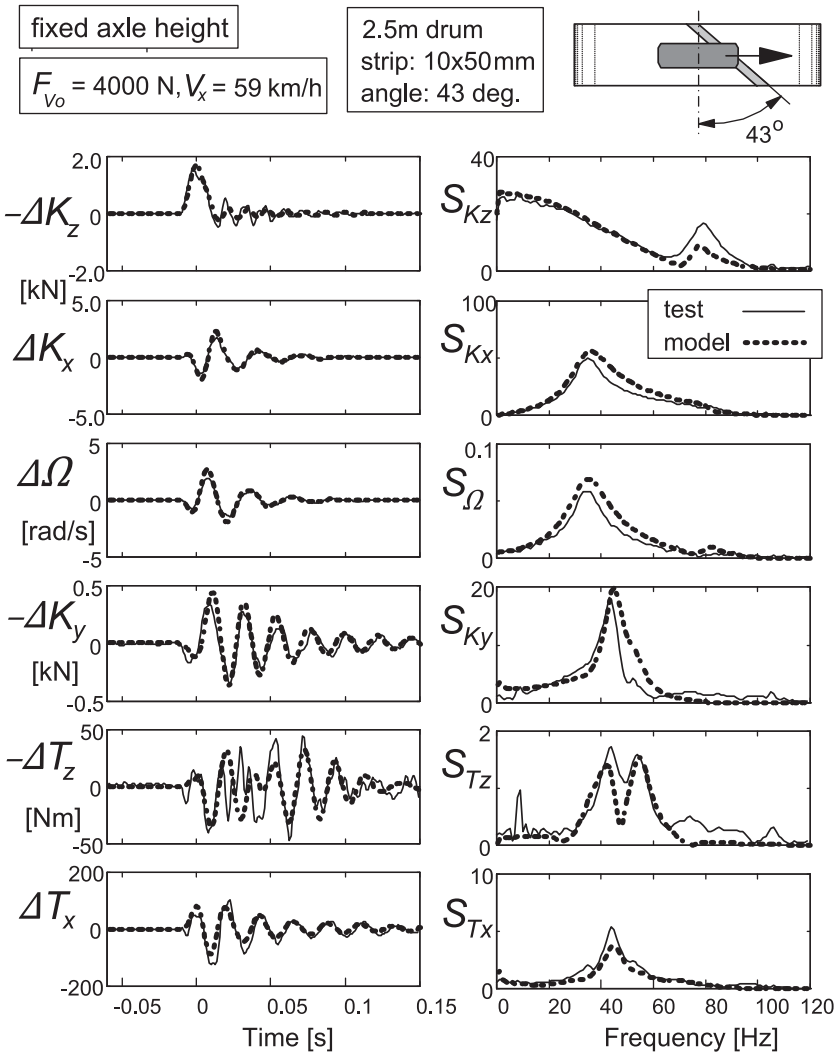

FIGURE 10.32 Running over an oblique cleat (10 × 50 mm strip) mounted on the drum surface at an angle of 43 degrees, at constant axle height. Measured and computed variations of wheel spindle forces K and moments T and wheel angular speed Ω versus time and as power spectral densities S.

wheel rolls over a pothole at a fixed axle location. The complex longitudinal force response conditions that are brought about by load and slip variations induced by tire modal vibrations and road unevennesses are simulated quite satisfactorily using the *SWIFT* model including obstacle geometric filtering.

10.2.2. Three-Dimensional Unevennesses

In Figure 10.32 example results are presented of experimental and model simulation results of the tire moving at constant axle height at a speed of 59 km/h over an oblique strip (height 10 mm, width 50 mm) mounted at an angle of 43 degrees with respect to the drum axis (wheel slip angle and wheel camber angle remain zero). The variations of the wheel spindle forces $K_{x,y,z}$ and moments $T_{x,z}$ and the wheel angular velocity Ω are presented as functions of time and as power spectral densities versus frequency. Note: The output forces and moments $K_{x,y,z}$ and $T_{x,z}$ are the same as the quantities $K_{a\xi,\eta,\zeta}$ and $T_{a\xi,\zeta}$ expressed by the Eqns (9.195–9.200), also cf. Figure 9.25.

Again, it is seen that a reasonable or good correspondence can be achieved. The various tire–wheel resonance frequencies can be observed to show up: vertical mode at 78 Hz (K_z), rotational mode at 35 Hz (K_x and Ω), camber mode at 46 Hz (K_y, T_z, and T_x), and yaw mode at 54 Hz (T_z).